

# Ultrafast optical currents in gapped graphene

S. Azar Oliaei Motlagh, Fatemeh Nematollahi, Aranyo Mitra, Jawad Zafar, Vadym Apalkov, and Mark I. Stockman

*Center for Nano-Optics (CeNO) and Department of Physics and Astronomy,  
Georgia State University, Atlanta, Georgia 30303, USA*

(Dated: November 19, 2021)

We study theoretically the interaction of ultrashort optical pulses with gapped graphene. Such strong pulse results in finite conduction band population and corresponding electric current both during and after the pulse. Since gapped graphene has broken inversion symmetry, it has an axial symmetry about the  $y$ -axis but not about the  $x$ -axis. We show that, in this case, if the linear pulse is polarized along the  $x$ -axis, the rectified electric current is generated in the  $y$  direction. At the same time, the conduction band population distribution in the reciprocal space is symmetric about the  $x$ -axis. Thus, the rectified current in gapped graphene has inter-band origin, while the intra-band contribution to the rectified current is zero.

## I. INTRODUCTION

The availability of ultrashort laser pulses with the duration of a few femtoseconds provides effective tools to manipulate and study the electron dynamics in solids at ultrafast time scale with high temporal resolution<sup>1–21</sup>. Among solids two dimensional (2D) crystalline materials exhibits unique properties due to the confinement of electron dynamics to a plane<sup>22</sup>. Graphene, a layer of carbon atoms with the thickness of one atom, is well known 2D material with fascinating properties. Graphene has a honeycomb crystal structure made of two sublattices, A and B - see Fig. 1(a)<sup>23,24</sup>. Having two Dirac points,  $K'$  and  $K$  at the edges of the Brillouin zone -see Fig. 1(b), makes graphene a suitable platform to study the dynamics of massless Dirac fermions<sup>22–25</sup>. In graphene, both time reversal and inversion symmetries are conserved. However, there is a broad class of semiconductors with honeycomb crystal structure where two sublattices are made of two different atoms, and the inversion symmetry is broken, which results in a finite bandgap at the  $K$  and  $K'$  points<sup>26,27</sup>. One of such materials is a monolayer of transition metal dichalcogenides (TMDCs) that has a direct bandgap with nonzero Berry curvature around the  $K'$  and  $K$  valleys. Gapped graphene, which has broken inversion symmetry, has topological properties similar to TMDC monolayer. Namely, the Berry curvature in gapped graphene is extended over the finite region near the  $K$  and  $K'$  points. Such broadening of the Berry curvature, which can be tuned by the bandgap, results in nontrivial topological properties of gapped graphene<sup>20,26,28,29</sup>. One of such properties is recently predicted topological resonance, which produces finite valley polarization in transition metal dichalcogenides and gapped graphene<sup>19</sup>.

In this article, we study the ultrafast nonlinear electron dynamics in gapped graphene. The dynamics is induced by a single cycle ultrafast linearly polarized pulse. Although the linear pulse does not produce any residual valley polarization, it results in electric current, the magnitude and the direction of which can be controlled by the bandgap. Gapped graphene, considered in the present article, is a model of direct bandgap semiconduc-

tors with honeycomb lattice structures. Opening of the bandgap in graphene can be achieved by several methods, for example, by placing graphene on Boron Nitride (BN) or silicon carbide (SiC) substrate<sup>30,31</sup>.

## II. MODEL AND MAIN EQUATIONS

In the presence of an applied ultrafast optical pulse,  $\mathbf{F}(t)$ , with the duration of less than 5 fs, the electron dynamics is coherent. This assumption is valid since the electron scattering time in 2D materials is longer than 10 fs<sup>32–37</sup>. To find the coherent electron dynamics in gapped graphene we solve time-dependent Schrödinger equation (TDSE)

$$i\hbar \frac{d\Psi}{dt} = H(t)\Psi, \quad (1)$$

with the Hamiltonian

$$H(t) = H_0 - e\mathbf{F}(t)\mathbf{r}, \quad (2)$$

where  $e$  is an electron charge, and  $H_0$  is the nearest neighbor tight binding Hamiltonian of gapped graphene<sup>38</sup>,

$$H_0 = \begin{pmatrix} \frac{\Delta}{2} & \gamma f(\mathbf{k}) \\ \gamma f^*(\mathbf{k}) & -\frac{\Delta}{2} \end{pmatrix}. \quad (3)$$

Here  $\Delta$  is the bandgap,  $\gamma = -3.03$  eV is the hopping integral, and

$$f(\mathbf{k}) = \exp\left(i\frac{ak_y}{\sqrt{3}}\right) + 2\exp\left(-i\frac{ak_y}{2\sqrt{3}}\right)\cos\left(\frac{ak_x}{2}\right), \quad (4)$$

where  $a = 2.46$  Å is a lattice constant. The eigenenergies of the tight-binding Hamiltonian,  $H_0$ , can be found as follows

$$E_c(\mathbf{k}) = +\sqrt{\gamma^2 |f(\mathbf{k})|^2 + \frac{\Delta^2}{4}}, \quad (5)$$

$$E_v(\mathbf{k}) = -\sqrt{\gamma^2 |f(\mathbf{k})|^2 + \frac{\Delta^2}{4}}, \quad (6)$$

where  $c$  and  $v$  stand for the conduction band (CB) and the valence band (VB), respectively. Figure 1(c) shows

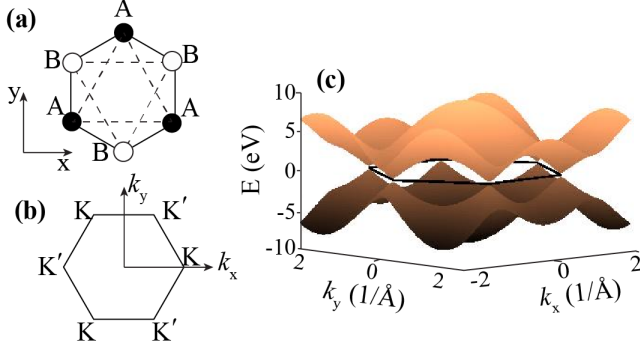


FIG. 1. (Color online) (a) The honeycomb lattice structure of graphene is made of two triangular sublattices A (black circle) and B (white circle). (b) The first Brillouin zone of the honeycomb lattice has two valleys  $K$  and  $K'$  located in its boundaries. (c) The energy dispersion is shown for gapped graphene with the bandgap of 0.5 eV in the extended zone. The solid black lines show the boundaries of the first Brillouin zone.

the calculated energy dispersion from Eqs. (5) and (6) for the bandgap of  $\Delta = 0.5$  eV.

The coherent electron dynamics in solids has two major components: intraband and interband dynamics. The intraband dynamics is governed by the Bloch acceleration theorem

$$\hbar \frac{d\mathbf{k}}{dt} = e\mathbf{F}(t). \quad (7)$$

The solution of this equation has the following form

$$\mathbf{k}(\mathbf{q}, t) = \mathbf{q} + \frac{e}{\hbar} \int_{-\infty}^t \mathbf{F}(t') dt', \quad (8)$$

where  $\mathbf{q}$  is the initial crystal wavevector of an electron in the first Brillouin zone.

The corresponding wave functions, which are the solutions of Schrödinger equation (1) within a single band  $\alpha$ , i.e., without interband coupling, are the Houston functions<sup>39</sup>,

$$\Phi_{\alpha\mathbf{q}}^{(H)}(\mathbf{r}, t) = \Psi_{\mathbf{k}(\mathbf{q}, t)}^{(\alpha)}(\mathbf{r}) \exp\left(i\phi_{\alpha}^{(d)}(\mathbf{q}, t) + i\phi_{\alpha}^{(B)}(\mathbf{q}, t)\right), \quad (9)$$

where  $\alpha = v, c$  stand for the VB and CB, respectively,  $\Psi_{\mathbf{k}}^{(\alpha)}$  are Bloch-band eigenstates in the absence of the external field,  $E_{\alpha}(\mathbf{k})$  are the eigenenergies, and the dynamic phase,  $\phi_{\alpha}^{(d)}$ , and geometric phase,  $\phi_{\alpha}^{(B)}$ , are defined as

$$\phi_{\alpha}^{(D)}(\mathbf{q}, t) = \frac{-1}{\hbar} \int_{-\infty}^t dt' (E_{\alpha}[\mathbf{k}(\mathbf{q}, t')]), \quad (10)$$

$$\phi_{\alpha}^{(B)}(\mathbf{q}, t) = \frac{e}{\hbar} \int_{-\infty}^t dt' \mathbf{F} \cdot (\mathcal{A}^{\alpha\alpha}[\mathbf{k}(\mathbf{q}, t')]). \quad (11)$$

Here  $\mathcal{A}^{\alpha\alpha} = \left\langle \Psi_{\mathbf{q}}^{(\alpha)} \left| i \frac{\partial}{\partial \mathbf{q}} \right| \Psi_{\mathbf{q}}^{(\alpha)} \right\rangle$  is the intraband Berry connection. The expressions for the intraband Berry con-

nections,  $\mathcal{A}^{\alpha\alpha} = (\mathcal{A}_x^{\alpha\alpha}, \mathcal{A}_y^{\alpha\alpha})$ , can be found from the tight-binding Hamiltonian as follows

$$\mathcal{A}_x^{\alpha\alpha}(\mathbf{k}) = \frac{-a\gamma^2}{\gamma^2|f(\mathbf{k})|^2 + (\Delta/2 - E_{\alpha})^2} \sin \frac{3ak_y}{2\sqrt{3}} \sin \frac{ak_x}{2}, \quad (12)$$

$$\mathcal{A}_y^{\alpha\alpha}(\mathbf{k}) = \frac{a\gamma^2}{\sqrt{3}(\gamma^2|f(\mathbf{k})|^2 + (\Delta/2 - E_{\alpha})^2)} \times \left( \cos ak_x - \cos \frac{\sqrt{3}ak_y}{2} \cos \frac{ak_x}{2} \right). \quad (13)$$

The interband electron dynamics is described by TDSE (1). The solution of TDSE can be expanded in the basis of Houston functions  $\Phi_{\alpha\mathbf{q}}^{(H)}(\mathbf{r}, t)$ <sup>40</sup>,

$$\Psi_{\mathbf{q}}(\mathbf{r}, t) = \sum_{\alpha=c,v} \beta_{\alpha\mathbf{q}}(t) \Phi_{\alpha\mathbf{q}}^{(H)}(\mathbf{r}, t), \quad (14)$$

where  $\beta_{\alpha\mathbf{q}}(t)$  are expansion coefficients, which satisfies the following system of coupled differential equations

$$i\hbar \frac{\partial B_{\mathbf{q}}(t)}{\partial t} = H'(\mathbf{q}, t) B_{\mathbf{q}}(t), \quad (15)$$

where the wave function (vector of state)  $B_{\mathbf{q}}(t)$  and Hamiltonian  $H'(\mathbf{q}, t)$  are defined as

$$B_{\mathbf{q}}(t) = \begin{bmatrix} \beta_{c\mathbf{q}}(t) \\ \beta_{v\mathbf{q}}(t) \end{bmatrix}, \quad (16)$$

$$H'(\mathbf{q}, t) = -e\mathbf{F}(t) \cdot \hat{\mathcal{A}}(\mathbf{q}, t), \quad (17)$$

$$\hat{\mathcal{A}}(\mathbf{q}, t) = \begin{bmatrix} 0 & \mathcal{D}^{cv}(\mathbf{q}, t) \\ \mathcal{D}^{vc}(\mathbf{q}, t) & 0 \end{bmatrix}. \quad (18)$$

where

$$\mathcal{D}^{cv}(\mathbf{q}, t) = \mathcal{A}^{cv}[\mathbf{k}(\mathbf{q}, t)] \times \exp\left(i\phi_{cv}^{(D)}(\mathbf{q}, t) + i\phi_{cv}^{(B)}(\mathbf{q}, t)\right), \quad (19)$$

$$\phi_{cv}^{(D)}(\mathbf{q}, t) = \phi_v^{(D)}(\mathbf{q}, t) - \phi_c^{(D)}(\mathbf{q}, t) \quad (20)$$

$$\phi_{cv}^{(B)}(\mathbf{q}, t) = \phi_v^{(B)}(\mathbf{q}, t) - \phi_c^{(B)}(\mathbf{q}, t) \quad (21)$$

$$\mathcal{A}^{cv}(\mathbf{q}) = \left\langle \Psi_{\mathbf{q}}^{(c)} \left| i \frac{\partial}{\partial \mathbf{q}} \right| \Psi_{\mathbf{q}}^{(v)} \right\rangle. \quad (22)$$

Here  $\mathcal{A}^{cv}(\mathbf{q})$  is a matrix element of the non-Abelian Berry connection<sup>41-43</sup>, which has the following expression

$$\mathcal{A}_x^{cv}(\mathbf{k}) = \mathcal{N} \left( \frac{-a}{2|f(\mathbf{k})|^2} \right) \left( \sin \frac{ak_x}{2} \sin \frac{a\sqrt{3}k_y}{2} + i \frac{\Delta}{2E_c} \left( \cos \frac{a\sqrt{3}k_y}{2} \sin \frac{ak_x}{2} + \sin ak_x \right) \right) \quad (23)$$

$$\mathcal{A}_y^{cv}(\mathbf{k}) = \mathcal{N} \left( \frac{a}{2\sqrt{3}|f(\mathbf{k})|^2} \right) \left( -1 - \cos \frac{a\sqrt{3}k_y}{2} \cos \frac{ak_x}{2} + 2 \cos^2 \frac{ak_x}{2} - i \frac{3\Delta}{2} E_c \sin \frac{a\sqrt{3}k_y}{2} \cos \frac{ak_x}{2} \right), \quad (24)$$

where

$$\mathcal{N} = \frac{|\gamma f(\mathbf{k})|}{\sqrt{\frac{\Delta^2}{4} + |\gamma f(\mathbf{k})|^2}}.$$

The ultrafast field drives electric current,  $\mathbf{J}(t) = \{J_x(t), J_y(t)\}$ . The current has both interband and intraband contributions,  $\mathbf{J}(t) = \mathbf{J}^{(\text{intra})}(t) + \mathbf{J}^{(\text{inter})}(t)$ . The intraband current is proportional to the group velocity and has the following form

$$\mathbf{J}^{(\text{intra})}(t) = \frac{eg_s}{a^2} \sum_{\alpha=c,v,\mathbf{q}} |\beta_\alpha(\mathbf{q}, t)|^2 \mathbf{v}^{(\alpha)}(\mathbf{k}(\mathbf{q}, t)), \quad (25)$$

where  $\mathbf{v}_{\mathbf{k}}^{(\alpha)} = \frac{\partial}{\partial \mathbf{k}} E^{(\alpha)}(\mathbf{k})$  is the group velocity (intraband velocity) and  $g_s = 2$  is the spin degeneracy. The group velocities can be found from Eqs. (5)-(6)

$$V_x^c(\mathbf{k}) = -V_x^v(\mathbf{k}) = \frac{-a\gamma^2}{\hbar\sqrt{|\gamma f(\mathbf{k})|^2 + \frac{\Delta^2}{4}}} \times \sin \frac{ak_x}{2} \left( \cos \frac{\sqrt{3}ak_y}{2} + 2 \cos \frac{ak_x}{2} \right) \quad (26)$$

$$V_y^c(\mathbf{k}) = -V_y^v(\mathbf{k}) = \frac{-\sqrt{3}a\gamma^2}{\hbar\sqrt{|\gamma f(\mathbf{k})|^2 + \frac{\Delta^2}{4}}} \times \sin \frac{\sqrt{3}ak_y}{2} \cos \frac{ak_x}{2}. \quad (27)$$

The interband current is given by the following expression

$$\begin{aligned} \mathbf{J}^{(\text{inter})}(t) &= i \frac{eg_s}{\hbar a^2} \sum_{\substack{\alpha, \alpha' = v, c \\ \alpha \neq \alpha'}} \beta_{\alpha'}^*(\mathbf{q}, t) \beta_\alpha(\mathbf{q}, t) \\ &\times \exp\{i\phi_{\alpha'\alpha}^{(\text{D})}(\mathbf{q}, t) + i\phi_{\alpha'\alpha}^{(\text{B})}(\mathbf{q}, t)\} \\ &\times [E_{\alpha'}(\mathbf{k}(\mathbf{q}, t)) - E_\alpha(\mathbf{k}(\mathbf{q}, t))] \mathcal{A}^{(\alpha\alpha')}(\mathbf{k}(\mathbf{q}, t)), \end{aligned} \quad (28)$$

where

$$\phi_{\alpha'\alpha}^{(\text{D})}(\mathbf{q}, t) = \phi_\alpha^{(\text{D})}(\mathbf{q}, t) - \phi_{\alpha'}^{(\text{D})}(\mathbf{q}, t), \quad (29)$$

$$\phi_{\alpha'\alpha}^{(\text{B})}(\mathbf{q}, t) = \phi_\alpha^{(\text{B})}(\mathbf{q}, t) - \phi_{\alpha'}^{(\text{B})}(\mathbf{q}, t). \quad (30)$$

### III. RESULTS AND DISCUSSION

In gapped graphene, sublattices *A* and *B* are unequivocal, which results in broken inversion symmetry. The gapped graphene is symmetric with respect to the *y*-axis, but there is no symmetry with respect to the *x*-axis, see Fig. 1. Thus, if the linear optical pulse is polarized along the *y*-axis, then the CB population distribution in the reciprocal space is symmetric with respect to the *y*-axis and the electric current is generated only along the *y*-axis, and not along the *x*-axis. But if the pulse is polarized along the *x*-axis, the current is expected to flow both along the *x* and *y* directions. Below we consider

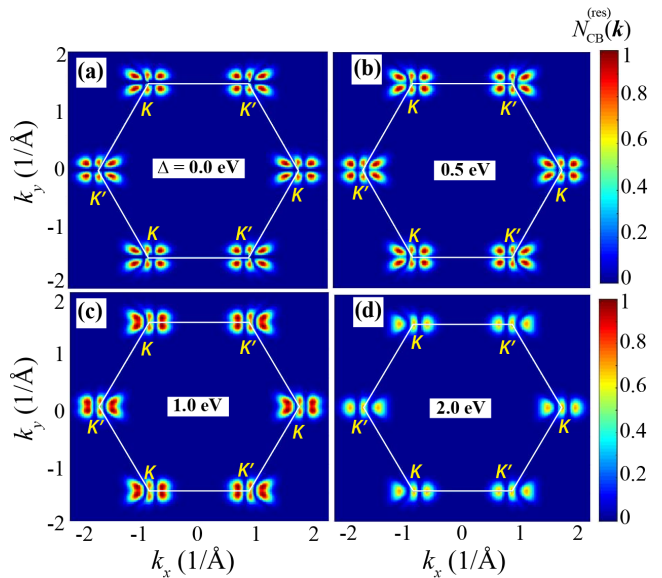


FIG. 2. (Color online) The residual CB population  $N_{\text{CB}}^{(\text{res})}(\mathbf{k})$  for gapped graphene with various bandgaps, 0 eV, 0.5 eV, 1 eV, and 2 eV, in the extended zone picture. The white solid line shows the boundaries of the first Brillouin zone with *K*, *K'*-points indicated. The applied field is linearly polarized pulse in the *x* direction and its amplitude is  $0.5 \text{ V \AA}^{-1}$ .

only this case, i.e., we assume that the optical pulse is polarized along the *x*-axis.

We consider a linearly *x*-polarized ultrafast optical pulse that is applied normally on the gapped graphene monolayer and has the following waveform

$$F = F_0(1 - 2u^2)e^{-u^2}, \quad (31)$$

where  $F_0$  is the amplitude of the pulse,  $u = t/\tau$ , and  $\tau = 1$  fs. We assume that the pulse is polarized along the *x*-axis. It should be mentioned that the *x*-axis is not the axis of symmetry of the gapped graphene, while the *y*-axis is the axis of symmetry.

In the presence of the pulse, we solve the TDSE assuming that the VB is initially occupied and the CB is empty. The electron dynamics in the field of the pulse is highly nonlinear and is characterized by redistribution of electrons between the valence and the conduction bands. After the pulse, there is a nonzero residual electron population,  $N_{\text{CB}}^{(\text{res})}$ , in the CB –see Fig. 2. Such population determines the irreversibility of the electron dynamics. The distributions of  $N_{\text{CB}}^{(\text{res})}$  in the reciprocal space are shown in Fig. 2(a)-(d) for different values of the band gap. The distributions are characterized by hot spots with large,  $\sim 1$ , CB population. Such hot spots are due to double passage of electrons of the *K* (*K'*) point during the pulse and the manifestation of interference pattern. Similar hot spots were discussed in Ref.44, where interaction of a linear optical pulse with pristine graphene has been studied. For gapped graphene, the interference

pattern becomes smeared, see Fig. 2. This is because the interband coupling is determined by non-Abelian Berry connection, the distribution of which is broadened with increasing the bandgap. At the same time, the separation between the fringes is inversely proportional to the nonlocality distance and, thus, does not depend on the bandgap<sup>44</sup>. Another interesting property of the CB population distribution is that it is symmetric with respect to both  $x$  and  $y$  axes. This is nontrivial property since the  $x$ -axis is not the axis of symmetry of the system.

The CB population distribution is shown in Fig. 3(a)-(d) at different moments of time. It illustrates the formation of the interference-induced hot spots in the CB population distribution. At all moments of time the CB population distribution is symmetric with respect to the  $x$  axis. Initially, at  $-2.5 \text{ fs} \leq t \leq -0.7 \text{ fs}$ , the applied field is negative so the electrons are accelerated to the right. Since the interband coupling is strong near the  $K$  and  $K'$  points only, the CB population within this time interval is large on left side of the Dirac points, see Fig. 3 (a).

For time interval  $-0.7 \text{ fs} \leq t \leq 0 \text{ fs}$ , the field is positive and the electrons move to the left and pass the Dirac points the second time, which results in interference fringes or hot spots on the left sides of the valleys as shown in Fig.3(b). The field remains positive for  $0 \text{ fs} \leq t \leq 0.7 \text{ fs}$  and now the electrons from the right side of the Dirac points pass the region near the  $K$  or  $K'$  points, which results in large CB population on the right side of the  $K$  and  $K'$  points, see Fig.3(c). The field changes its sign at  $0.7 \text{ fs} \leq t \leq 2.5 \text{ fs}$ . Then the electrons from the right side of the Dirac points pass through the region of large interband coupling the second time, which produce hot spots of CB population on the right side of the  $K$  and  $K'$  points. The electron CB distributions shown in Figs. 2 and 3 could be observed by the time resolve angle-resolved photoelectron spectroscopy (tr-ARPES)<sup>45,46</sup>.

Redistribution of electrons between the VB and CB during the pulse generates an electric current. For the pulse polarized along the  $x$ -axis, which is not the axis of symmetry for the gapped graphene, both the longitudinal current, i.e., the current in the  $x$  direction, and the transverse current, i.e., the current in the  $y$  direction, are generated. Such currents are shown in Fig. 4 for different values of the bandgap,  $\Delta$ . For zero bandgap, i.e., for pristine graphene, the transverse current is zero. The transverse current increases with the bandgap. The electric current, generated during the pulse, has two contributions: intraband and interband. The intraband current is completely determined by the electron density distributions in the CB and VB. It can be also considered as a measure of asymmetry of such distributions. Such the CB population distribution is symmetric with respect to the  $y$ -axis both during the pulse and after the pulse, the intraband transverse current,  $J_y$ , is zero. Thus, the transverse current for gapped graphene is determined by the interband contribution only. As the results, the trans-

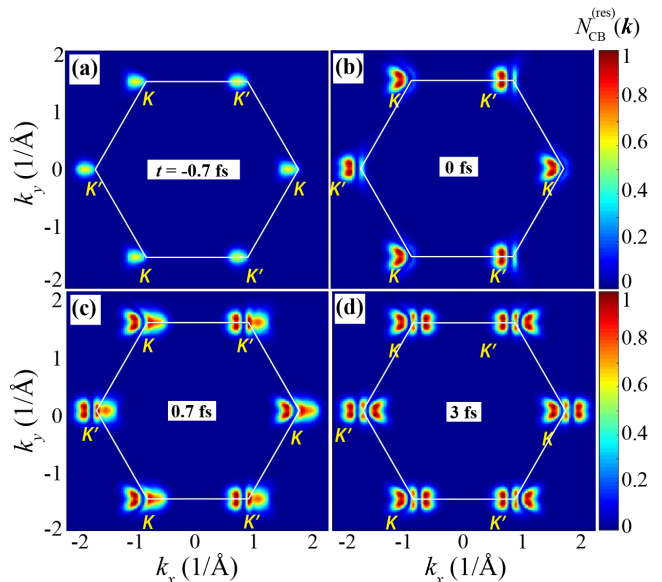


FIG. 3. (Color online) The CB population  $N_{\text{CB}}(\mathbf{k})$  as a function of initial lattice vector for gapped graphene with bandgap 1 eV in the extended zone picture at different moments of time, -0.7 fs, 0 fs, 0.7 fs, and 3 fs. The white solid line shows the boundaries of the first Brillouin zone with  $K, K'$ -points indicated. The applied pulse is linearly polarized in the  $x$  direction and its amplitude is  $0.5 \text{ V\AA}^{-1}$ .

verse current as a function of time is oscillating with the frequency that depends on the bandgap, see Fig. 4(a). At the same time, the longitudinal current is almost unidirectional with small oscillations, see Fig. 4(b).

Since the bandgap determines the strength of the asymmetry of the system, we expect that the magnitude of the transverse current increases with the bandgap, which is shown in Fig. 4(a). For the longitudinal current, there is a different tendency. The longitudinal current first increases with  $\Delta$  and then at large bandgaps,  $\Delta \sim 2eV$ , decreases. Such suppression of the longitudinal current at large values of  $\Delta$  is due to the specific dependence of the interband dipole matrix elements (non-Abelian Berry connection) on the bandgap. At small bandgaps, the interband dipole matrix element is strongly localized near the  $K$  and  $K'$  points. With increasing the bandgap, the dipole matrix element becomes delocalized and nonzero at large part of the Brillouin zone, where the maximum of the dipole matrix element decreases with the bandgap keeping the net dipole matrix element, i.e., the integral of the dipole matrix element over the whole Brillouin zone, constant. As a results the total CB population near the  $K$  or  $K'$  points decreases with  $\Delta$ , which finally results in suppression of the longitudinal current.

In Fig. 5 the longitudinal and transverse currents are shown for different field amplitudes. As expected, with increasing the field amplitude, the magnitudes of both currents increase. The frequency of oscillations of the

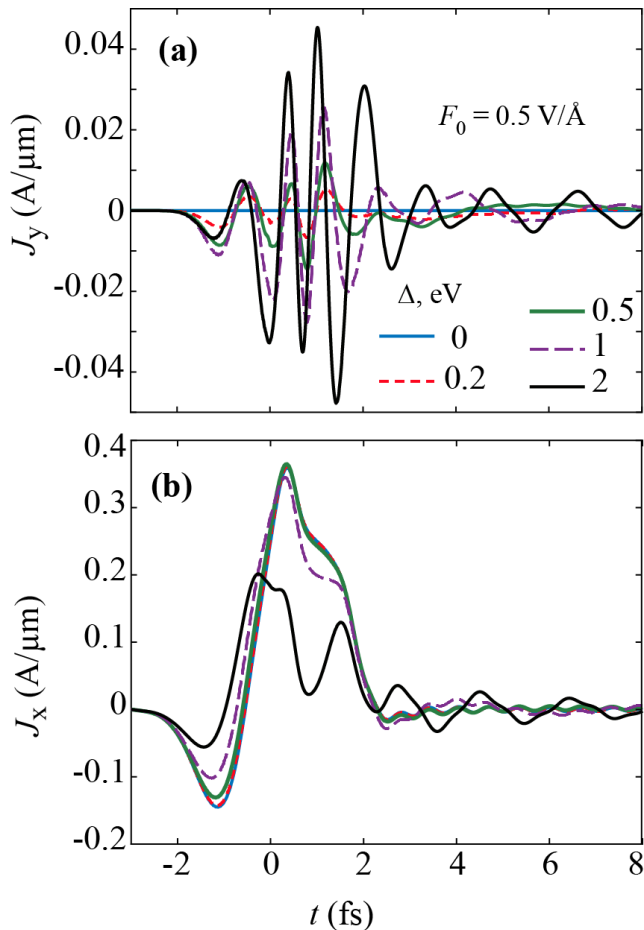


FIG. 4. The current densities in gapped graphene are shown as a function of time for various bandgaps, 0 eV, 0.2 eV, 0.5 eV, 1 eV, and 2 eV. (a) The current density,  $J_y$ , is in the direction of normal to the applied field. (b) The current density,  $J_x$ , is along the direction of the applied field. The applied pulse is linearly polarized in the  $x$  direction and its amplitude is  $0.5 \text{ V}\text{\AA}^{-1}$ .

transverse current also shows the dependence on the magnitude of the pulse, while the longitudinal current is almost unidirectional.

The direction of the current is determined by the direction of the field maximum. For the field profile (31), the field maximum is pointing in the positive direction of the  $x$ -axis. If we change the direction of the field maximum to the negative one, i.e., it is pointing in the negative direction of the  $x$ -axis, then the longitudinal current,  $J_x$ , changes its sign, while the transverse current,  $J_y$ , remains the same. The transverse current changes its sign if we change the signs of the on-site energies of sublattices  $A$  and  $B$ , i.e., change the sign of parameter  $\Delta$  in Hamiltonian (3).

The generated electric current during the pulse results in the transfer of an electric charge through the system.

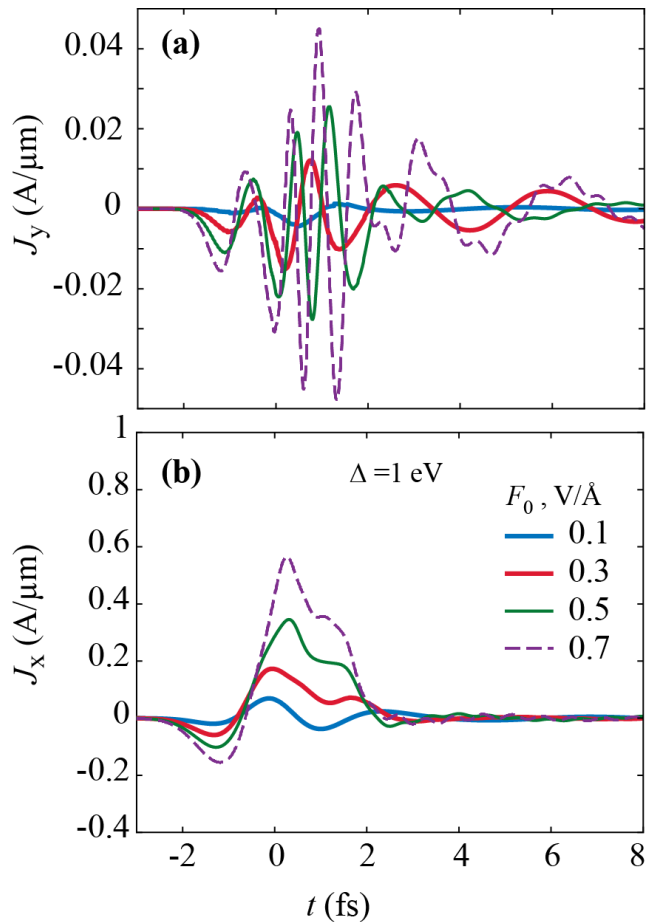


FIG. 5. The current densities in gapped graphene are shown as a function of time for various field's amplitudes,  $0.1 \text{ V}\text{\AA}^{-1}$ ,  $0.3 \text{ V}\text{\AA}^{-1}$ ,  $0.5 \text{ V}\text{\AA}^{-1}$ , and  $0.7 \text{ V}\text{\AA}^{-1}$ . (a) The current density,  $J_y$ , is in the direction of normal to the applied field. (b) The current density,  $J_x$ , is along the direction of the applied field. The applied pulse is linearly polarized in the  $x$  direction and the bandgap of gapped graphene is 1 eV.

Such transferred charge can be calculated as

$$\mathbf{Q} = \int_{-\infty}^{\infty} \mathbf{J}(t) dt. \quad (32)$$

For the pulse polarized along the  $x$ -axis, the charge is transferred in both  $x$  and  $y$  directions. In Fig. 6 the transferred charge is shown as a function of the pulse amplitude for different values of the bandgap. As expected, for zero bandgap, there is no charge transfer in the transverse direction,  $Q_y = 0$ . As a function of the field amplitude, the transverse transferred charge shows oscillations, which is due to oscillations in the transverse current as a function of time. The longitudinal transferred charge,  $Q_x$ , monotonically increases with the field amplitude and has weak dependence on the bandgap. At large bandgap,  $\Delta \sim 2 \text{ eV}$ , transferred charge  $Q_x$  becomes smaller, which is related to suppression of the CB population and correspondingly the longitudinal electric current

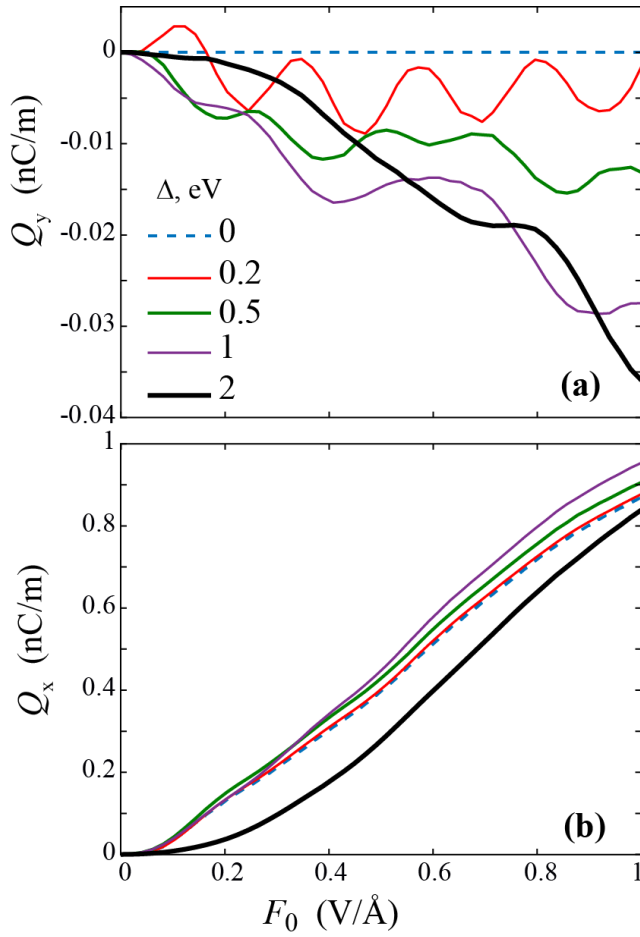


FIG. 6. The transferred charge densities are shown as a function of the field amplitude,  $F_0$ , for different bandgaps, 0 eV (case of graphene), 0.2 eV, 0.5 eV, 1 eV, and 2 eV. (a) The transferred charge density is shown in the direction normal to the applied field,  $Q_y$ , and (b) The transferred charge density is shown along the direction of the field,  $Q_x$ . The applied pulse is linearly polarized in the x direction.

at large  $\Delta$ .

Changing the direction of the applied field and applying it in -x direction changes the sign of the longitudinal current however, it does not have any effect on the normal current. This current only changes the sign if we change the on-site energies of different sublattices.

#### IV. CONCLUSION

In pristine graphene, which has an inversion symmetry, there are two axes of symmetry, say  $x$  and  $y$ . If an external linear pulse is polarized along these two directions, then it will produce CB population distribution that is

symmetric with respect to the axis of polarization of the pulse. The pulse will also generate an electric current and the corresponding transferred charge along the direction of polarization only, but not in the transverse direction.

For gapped graphene, the inversion symmetry is broken. In this case there is only one axis of symmetry, say the  $y$ -axis. If the linear pulse is polarized along the  $x$  axis, then since this axis is not the axis of symmetry, the electric current is generated in both  $x$  and  $y$  directions. The transverse current does not depend on the direction of the field maximum, while the longitudinal current changes its sign when the direction of the maximum is reversed. At the same time, for the same polarization of the pulse, i.e., along the  $x$ -axis, similar to pristine graphene, the CB population distribution is symmetric with respect to the  $x$ -axis both during the pulse and after the pulse. It means that the electron dynamics above ( $k_y > 0$ ) and below ( $k_y < 0$ ) the  $K$  ( $K'$ ) point is exactly the same, which results in symmetric CB population distribution. Although the electron dynamics depends on the geometric phase, which is different above and below the  $K$  ( $K'$ ) point, this phase is exactly canceled by the phase of the interband dipole matrix element (non-Abelian Berry connection). This is the property of the two-band model of gapped graphene which will be discussed somewhere else. If more bands are included into the model, then there will be no cancellation of the geometric phase and the net (topological) phase, which is the sum of the geometric phase and the phase of the interband dipole coupling, will be nonzero. The topological phase has different time dependence above and below the  $K$  ( $K'$ ), which results in topological resonance. The topological resonance occurs due to a partial cancellation of the dynamic phase by the topological phase. Such partial cancellation is different above and below the  $K$  ( $K'$ ) point, which finally results in different CB populations and asymmetric CB population distribution. Such small asymmetry of CB population will introduce small intraband contribution to the transverse current.

#### ACKNOWLEDGMENTS

Major funding was provided by Grant No. DE-FG02-11ER46789 from the Materials Sciences and Engineering Division of the Office of the Basic Energy Sciences, Office of Science, U.S. Department of Energy. Numerical simulations have been performed using support by Grant No. DE-FG02-01ER15213 from the Chemical Sciences, Biosciences and Geosciences Division, Office of Basic Energy Sciences, Office of Science, US Department of Energy. The work of V.A. was supported by NSF EFRI NewLAW Grant EFMA-17 41691. Support for S.A.O.M. came from a MURI Grant No. FA9550-15-1-0037 from the US Air Force of Scientific Research.

- <sup>1</sup> A. Schiffrin, T. Paasch-Colberg, N. Karpowicz, V. Apalkov, D. Gerster, S. Muhlbrandt, M. Korbman, J. Reichert, M. Schultze, S. Holzner, J. V. Barth, R. Kienberger, R. Ernstorfer, V. S. Yakovlev, M. I. Stockman, and F. Krausz, "Optical-field-induced current in dielectrics," *Nature* **493**, 70–74 (2012).
- <sup>2</sup> V. Apalkov and M. I. Stockman, "Theory of dielectric nanofilms in strong ultrafast optical fields," *Phys. Rev. B* **86**, 165118–1–13 (2012).
- <sup>3</sup> T. Higuchi, C. Heide, K. Ullmann, H. B. Weber, and P. Hommelhoff, "Light-field-driven currents in graphene," *Nature* **550**, 224–228 (2017).
- <sup>4</sup> Elisabeth Gruber, Richard A. Wilhelm, Rmi Ptuya, Valerie Smejkal, Roland Kozubek, Anke Hierzenberger, Bernhard C. Bayer, Iigo Aldazabal, Andrey K. Kazansky, Florian Libisch, Arkady V. Krasheninnikov, Marika Schleberger, Stefan Fackso, Andrei G. Borisov, Andrs Arnau, and Friedrich Aumayr, "Ultrafast electronic response of graphene to a strong and localized electric field," *Nature Communications* **7**, 13948 (2016).
- <sup>5</sup> S. A. Oliaei Motlagh, V. Apalkov, and M. I. Stockman, "Interaction of crystalline topological insulator with an ultrashort laser pulse," *Phys. Rev. B* **95**, 085438–1–8 (2017).
- <sup>6</sup> S. A. O. Motlagh, J. S. Wu, V. Apalkov, and M. I. Stockman, "Fundamentally fastest optical processes at the surface of a topological insulator," *Physical Review B* **98**, 125410–1–11 (2018).
- <sup>7</sup> F. Nematollahi, S. A. O. Motlagh, V. Apalkov, and M. I. Stockman, "Weyl semimetals in ultrafast laser fields," *Physical Review B* **99**, 245409–1–9 (2019).
- <sup>8</sup> C. Heide, T. Higuchi, H. B. Weber, and P. Hommelhoff, "Coherent electron trajectory control in graphene," *Phys. Rev. Lett.* **121**, 207401–1–5 (2018).
- <sup>9</sup> Yong Sing You, Yanchun Yin, Yi Wu, Andrew Chew, Xiaoming Ren, Fengjiang Zhuang, Shima Gholam-Mirzaei, Michael Chini, Zenghu Chang, and Shambhu Ghimire, "High-harmonic generation in amorphous solids," *Nature Communications* **8**, 724 (2017).
- <sup>10</sup> H. Z. Liu, Y. L. Li, Y. S. You, S. Ghimire, T. F. Heinz, and D. A. Reis, "High-harmonic generation from an atomically thin semiconductor," *Nat. Phys.* **13**, 262–266 (2017).
- <sup>11</sup> A. Kaiser, B. Rethfeld, M. Vicanek, and G. Simon, "Microscopic processes in dielectrics under irradiation by subpicosecond laser pulses," *Phys. Rev. B* **61**, 11437–11450 (2000).
- <sup>12</sup> Christian Heide, Tobias Boolakee, Takuya Higuchi, Heiko B. Weber, and Peter Hommelhoff, "Interaction of carrier envelope phase-stable laser pulses with graphene: the transition from the weak-field to the strong-field regime," *arXiv e-prints*, arXiv:1903.07558 (2019), arXiv:1903.07558 [physics.optics].
- <sup>13</sup> Dong Sun, Grant Aivazian, Aaron M. Jones, Jason S. Ross, Wang Yao, David Cobden, and Xiaodong Xu, "Ultrafast hot-carrier-dominated photocurrent in graphene," *Nature Nanotechnology* **7**, 114 (2012).
- <sup>14</sup> Hiroki Mashiko, Yuta Chisuga, Ikufumi Katayama, Katsuya Oguri, Hiroyuki Masuda, Jun Takeda, and Hideki Gotoh, "Multi-petahertz electron interference in cr:al2o3 solid-state material," *Nature Communications* **9**, 1468 (2018).
- <sup>15</sup> Hee Jun Shin, Van Luan Nguyen, Seong Chu Lim, and Joo-Hiuk Son, "Ultrafast nonlinear travel of hot carriers driven by high-field terahertz pulse," *Journal of Physics B: Atomic, Molecular and Optical Physics* **51**, 144003 (2018).
- <sup>16</sup> Takuya Higuchi, Christian Heide, Konrad Ullmann, Heiko B. Weber, and Peter Hommelhoff, "Light-field-driven currents in graphene," *Nature* **550**, 224–228 (2017).
- <sup>17</sup> M. Trushin, A. Grupp, G. Soavi, A. Budweg, D. De Fazio, U. Sassi, A. Lombardo, A. C. Ferrari, W. Belzig, A. Leitenstorfer, and D. Brida, "Ultrafast pseudospin dynamics in graphene," *Phys. Rev. B* **92**, 165429 (2015).
- <sup>18</sup> H. Koochaki Keldarreh, V. Apalkov, and M. I. Stockman, "Graphene superlattices in strong circularly polarized fields: Chirality, Berry phase, and attosecond dynamics," *Phys. Rev. B* **96**, 075409–1–8 (2017).
- <sup>19</sup> S. A. Oliaei Motlagh, J.-S. Wu, V. Apalkov, and M. I. Stockman, "Femtosecond valley polarization and topological resonances in transition metal dichalcogenides," *Phys. Rev. B* **98**, 081406(R)–1–6 (2018).
- <sup>20</sup> D. Sun, J. W. Lai, J. C. Ma, Q. S. Wang, and J. Liu, "Review of ultrafast spectroscopy studies of valley carrier dynamics in two-dimensional semiconducting transition metal dichalcogenides," *Chinese Physics B* **26** (2017), Artn 037801 10.1088/1674-1056/26/3/037801.
- <sup>21</sup> Jun Zhang, Hao Ouyang, Xin Zheng, Jie You, Runze Chen, Tong Zhou, Yizhen Sui, Yu Liu, Xiang'ai Cheng, and Tian Jiang, "Ultrafast saturable absorption of mos2 nanosheets under different pulse-width excitation conditions," *Opt. Lett.* **43**, 243–246 (2018).
- <sup>22</sup> S. Z. Butler, S. M. Hollen, L. Y. Cao, Y. Cui, J. A. Gupta, H. R. Gutierrez, T. F. Heinz, S. S. Hong, J. X. Huang, A. F. Ismach, E. Johnston-Halperin, M. Kuno, V. V. Plashnitsa, R. D. Robinson, R. S. Ruoff, S. Salahuddin, J. Shan, L. Shi, M. G. Spencer, M. Terrones, W. Windl, and J. E. Goldberger, "Progress, challenges, and opportunities in two-dimensional materials beyond graphene," *Acc Nano* **7**, 2898–2926 (2013).
- <sup>23</sup> A. K. Geim and K. S. Novoselov, "The rise of graphene," *Nat Mater* **6**, 183–191 (2007).
- <sup>24</sup> A. H. Castro Neto, F. Guinea, N. M. R. Peres, K. S. Novoselov, and A. K. Geim, "The electronic properties of graphene," *Rev. Mod. Phys.* **81**, 109–162 (2009).
- <sup>25</sup> K. S. Novoselov, A. K. Geim, S. V. Morozov, D. Jiang, M. I. Katsnelson, I. V. Grigorieva, S. V. Dubonos, and A. A. Firsov, "Two-dimensional gas of massless Dirac fermions in graphene," *Nature* **438**, 197–200 (2005).
- <sup>26</sup> A. Kormanyos, G. Burkard, M. Gmitra, J. Fabian, V. Zolyomi, N. D. Drummond, and V. Fal'ko, "k.p theory for two-dimensional transition metal dichalcogenide semiconductors (vol 2, 022001, 2015)," *2d Materials* **2** (2015).
- <sup>27</sup> J. W. Jiang, "Graphene versus MoS<sub>2</sub>: A short review," *Frontiers of Physics* **10**, 287–302 (2015).
- <sup>28</sup> Y. Ye, J. Xiao, H. L. Wang, Z. L. Ye, H. Y. Zhu, M. Zhao, Y. Wang, J. H. Zhao, X. B. Yin, and X. Zhang, "Electrical generation and control of the valley carriers in a monolayer transition metal dichalcogenide," *Nature Nanotechnology* **11**, 598–602 (2016).
- <sup>29</sup> D. Jariwala, V. K. Sangwan, L. J. Lauhon, T. J. Marks, and M. C. Hersam, "Emerging device applications for semiconducting two-dimensional transition metal dichalcogenides," *Acc Nano* **8**, 1102–1120 (2014).
- <sup>30</sup> M. S. Nevius, M. Conrad, F. Wang, A. Celis, M. N. Nair,

- A. Taleb-Ibrahimi, A. Tejada, and E. H. Conrad, “Semiconducting graphene from highly ordered substrate interactions,” *Phys. Rev. Lett.* **115**, 136802 (2015).
- <sup>31</sup> D. Jariwala, A. Srivastava, and P. M. Ajayan, “Graphene synthesis and band gap opening,” *J. Nanosci. Nanotechnol.* **11**, 6621–6641 (2011).
- <sup>32</sup> E. H. Hwang and S. Das Sarma, “Single-particle relaxation time versus transport scattering time in a two-dimensional graphene layer,” *Phys. Rev. B* **77**, 195412–1–6 (2008).
- <sup>33</sup> M. Breusing, S. Kuehn, T. Winzer, E. Malic, F. Milde, N. Severin, J. P. Rabe, C. Ropers, A. Knorr, and T. Elsaesser, “Ultrafast nonequilibrium carrier dynamics in a single graphene layer,” *Physical Review B* **83**, 153410 (2011).
- <sup>34</sup> Ermin Malic, Torben Winzer, Evgeny Bobkin, and Andreas Knorr, “Microscopic theory of absorption and ultrafast many-particle kinetics in graphene,” *Phys. Rev. B* **84**, 205406 (2011).
- <sup>35</sup> D. Brida, A. Tomadin, C. Manzoni, Y. J. Kim, A. Lombardo, S. Milana, R. R. Nair, K. S. Novoselov, A. C. Ferrari, G. Cerullo, and M. Polini, “Ultrafast collinear scattering and carrier multiplication in graphene,” *Nat Commun* **4**, 1987–1–9 (2013).
- <sup>36</sup> I. Gierz, J. C. Petersen, M. Mitran, C. Cacho, I. C. Turcu, E. Springate, A. Stohr, A. Kohler, U. Starke, and A. Cavalleri, “Snapshots of non-equilibrium Dirac carrier distributions in graphene,” *Nat. Mater.* **12**, 1119–24 (2013).
- <sup>37</sup> Andrea Tomadin, Daniele Brida, Giulio Cerullo, Andrea C. Ferrari, and Marco Polini, “Nonequilibrium dynamics of photoexcited electrons in graphene: Collinear scattering, Auger processes, and the impact of screening,” *Phys. Rev. B* **88**, 035430 (2013).
- <sup>38</sup> Thomas G. Pedersen, Antti-Pekka Jauho, and Kjeld Pedersen, “Optical response and excitons in gapped graphene,” *Phys. Rev. B* **79**, 113406 (2009).
- <sup>39</sup> W. V. Houston, “Acceleration of electrons in a crystal lattice,” *Phys. Rev.* **57**, 184–186 (1940).
- <sup>40</sup> W. V. Houston, “Acceleration of electrons in a crystal lattice,” *Phys. Rev.* **57**, 184–186 (1940).
- <sup>41</sup> F. Wilczek and A. Zee, “Appearance of gauge structure in simple dynamical systems,” *Phys. Rev. Lett.* **52**, 2111–2114 (1984).
- <sup>42</sup> D. Xiao, M.-C. Chang, and Q. Niu, “Berry phase effects on electronic properties,” *Reviews of Modern Physics* **82**, 1959–2007 (2010).
- <sup>43</sup> F. Yang and R. B. Liu, “Nonlinear optical response induced by non-Abelian Berry curvature in time-reversal-invariant insulators,” *Phys. Rev. B* **90**, 245205 (2014).
- <sup>44</sup> H. K. Kelardeh, V. Apalkov, and M. I. Stockman, “Graphene in ultrafast and superstrong laser fields,” *Phys. Rev. B* **91**, 045439–1–8 (2015).
- <sup>45</sup> Y. Liu, G. Bian, T. Miller, and T. C. Chiang, “Visualizing electronic chirality and Berry phases in graphene systems using photoemission with circularly polarized light,” *Phys. Rev. Lett.* **107**, 166803–1–5 (2011).
- <sup>46</sup> A. F. Kemper, M. A. Sentef, B. Moritz, T. P. Devereaux, and J. K. Freericks, “Review of the theoretical description of time-resolved angle-resolved photoemission spectroscopy in electron-phonon mediated superconductors,” *Ann. Phys.-Berlin* **529**, 1600235–1–11 (2017).